HHS Public Access

Author manuscript

Mol Imaging Biol. Author manuscript; available in PMC 2017 March 09.

Published in final edited form as:

Mol Imaging Biol. 2014 October ; 16(5): 730–738. doi:10.1007/s11307-014-0779-3.

Human Brain Imaging of α7 nAChR with [^{18}F]ASEM: a New PET Radiotracer for Neuropsychiatry and Determination of Drug Occupancy

Dean F. Wong[1,2,3,4,5], **Hiroto Kuwabara**[1], **Martin Pomper**[1,2,4], **Daniel P. Holt**[1], **James R. Brasic**[1], **Noble George**[1], **Boris Frolov**[1], **William Willis**[1], **Yongjun Gao**[1], **Heather Valentine**[1], **Ayon Nandi**[1], **Lorena Gapasin**[1], **Robert F. Dannals**[1,4], and **Andrew G. Horti**[1]

[1]Department of Radiology, School of Medicine, The Johns Hopkins University, Baltimore, MD, USA

[2]Department of Psychiatry, School of Medicine, The Johns Hopkins University, Baltimore, MD, USA

[3]Department of Neuroscience, School of Medicine, The Johns Hopkins University, Baltimore, MD, USA

[4]Department of Environmental Health Sciences, Bloomberg School of Public Health, The Johns Hopkins University, Baltimore, MD, USA

[5]Johns Hopkins Medical Institutions, JHOC Bldg. Room 3245, 601 N. Caroline St., Baltimore, MD, 21287, USA

Abstract

Purpose—Using the α7-nAChR radiotracer, [^{18}F]ASEM, we present the first successful human positron emission tomography (PET) studies. Rodent occupancy with three clinically employed α7-nAChR drugs confirms the specificity of the radiotracer.

Procedures—Five healthy male subjects were imaged for 90 min following IV [^{18}F]ASEM. Two subjects were scanned for the second time (test/retest; TRV). Mouse biodistribution of [^{18}F]ASEM was carried out in CD1 mice injected with using human equivalent doses of DMXB-A, EVP-6124, and varenicline to block specific binding.

Results—[^{18}F]ASEM readily entered the brain and peaked at 15 min post-injection with reversible kinetics and a peak %SUV of about 400 %. The regional human brain distribution of [^{18}F]ASEM matched previous ***in vitro*** data and baboon PET results. The precuneus, parietal, occipital, cingulate cortexes, putamen, and thalamus showed high values of distribution volume (>20 ml/ml) and binding potentials >1 with TRV averaged 10.8±5.1 %. In mouse distribution studies, there was significant dose-dependent blockade in the mouse brain with DMXB-A as well as the other two α7-nAChR drugs.

Correspondence to: Dean Wong; dfwong@jhmi.edu.

Electronic supplementary material The online version of this article (doi:10.1007/s11307-014-0779-3) contains supplementary material, which is available to authorized users.

Conflict of Interest. The authors declare that they have no conflict of interest.

Conclusions—The characteristics of [^{18}F]ASEM are consistent with the ability to quantify α7-nAChR in the human brain. [^{18}F]ASEM is suitable for imaging neuropsychiatric disorders and target engagement (receptor occupancy) of potential α7-nAChR drugs.

Keywords

Alpha-7; Nicotinic acetylcholine receptor; DMXB-A; GTS-21; Schizophrenia; Receptor occupancy; Radiotracer kinetic modeling; PET brain imaging

Introduction

Nicotinic acetylcholine receptors (nAChRs) are ligand-gated ion channels distributed throughout the peripheral and central nervous systems (CNS) and non-neuronal cells [1]. Various subtypes of cerebral nAChR are mostly comprised of the α4β2- and α7-nAChR subtypes. The α7-nAChR subtype that is permeable to Ca^{2+}, Na^{+}, and K^{+} ions has been implicated in the pathophysiology of psychiatric disorders, Alzheimer's disease (AD), traumatic brain injury, multiple sclerosis, neuroinflammation, and tobacco smoking addiction [1–7] as well as various non-CNS conditions and diseases [8], but the complete role of α7-nAChR in the CNS has not been discovered. Altered density of cerebral α7-nAChRs has been seen post-mortem in patients with schizophrenia (SCZ) [9, 10] and bipolar disorder [11]. The α7-nAChR subtype is important in thinking processes, and it is highly expressed in the human hippocampus and cortex regions that are involved in cognition and memory (see review [12]).

The critical role of α7-nAChRs in human physiology has recently been supported by clinical studies with α7-nAChR agonists—emerging drugs for treatment of cognitive dysfunction (see for review [13, 14]). However, positron emission tomography (PET) imaging of the α7-nAChR has not been possible in human subjects due to the unavailability of suitable radioligands with sufficient specific binding.

Development of a PET radioligand for α7-nAChR is a challenge because this receptor exhibits moderate concentration in the CNS (0.3–15 fmol/mg protein in humans [10] and non-human primates [15, 16]). A successful PET radioligand for α7-nAChR must exhibit a combination of picomolar binding affinity, high selectivity, and other essential characteristics [17]. Recent reviews describe considerable, but mostly unsuccessful, efforts of several research groups to develop an α7-nAChR PET radioligand [17–19]. A number of α7-nAChR radioligands have been synthesized for PET and single photon emission computed tomography (Supplemental Fig. 1) [20–30]. Unfortunately, the previous radioligands did not manifest suitably high specific binding at α7-nAChR *in vivo*. There is still a pressing need for a high specific uptake PET radiotracer for quantification of α7-nAChRs in humans.

[^{11}C]CHIBA-1001 (Supplemental Fig. 1), the only α7-nAChR radioligand that had been studied with human PET, showed relatively low target-to-non-target ratios in the brain regions (<1.3) in a single human experiment. No further PET studies have been reported after the initial publication [27]. In monkey PET studies, [^{11}C]CHIBA-1001 demonstrated high brain uptake in the cortexes, striatum, hippocampus, and thalamus and lower uptake in

the cerebellum [21]. In the same monkey PET study, injection of SSR180711, a selective partial α7-nAChR agonist, demonstrated a reduction (25–30 %) of [^{11}C]CHIBA-1001 radioactivity in the high uptake regions. Further *in vitro* binding studies with [^{3}H]CHIBA-1001 showed a relatively low equilibrium dissociation constant (rat K_D=193 nM) and a distribution of binding to crude membranes from dissected brain regions of rat, monkeys, and human that did not match the known distribution of α7-nAChRs [31]. Furthermore, researchers from AstraZeneca showed that [^{3}H]CHIBA-1001 exhibited low *in vitro* binding affinity (rat hippocampus or human α7-nAChR recombinant membranes, K_D =120–180 nM) and poor α7-nAChR regional and pharmacological selectivity in the rodent brain [32], confirming the relatively poor PET imaging properties of [^{11}C]CHIBA-1001.

Recently, we synthesized a new, selective α7-nAChR PET radioligand [^{18}F]ASEM (Fig. 1), with subnanomolar binding affinity [33]. [^{18}F]ASEM readily entered the mouse [33] and baboon brain [34] and selectively labeled α7-nAChR with high α7-nAChR specificity in both animal species. [^{18}F]ASEM is currently the only α7-nAChR PET radioligand with suitable properties for quantitative PET imaging of α7-nAChR in the animal brain.

We now report the first human PET with [^{18}F]ASEM making it feasible to image neuropsychiatric disorders including SCZ and to quantify target engagement of α7-nAChR therapeutic drugs. To that end, the occupancy of rodent α7-nAChR receptors is documented for α7-nAChR drugs that are currently in clinical trials in SCZ and other disorders (Presented in part at the Neuroreceptor Mapping Conference NRM14, Amsterdam, Netherlands, May 2014).

Materials and Methods

Radiosynthesis of [^{18}F]ASEM for Human Studies

[^{18}F]ASEM for human studies was synthesized by an efficient onestep microwave radiosynthesis *via* the corresponding nitro-precursor [33]. The synthesis provided the final radiotracer product in a good radiochemical yield (20.1±8.9 %, n=6) and high radiochemical purity (98±1 %) and specific radioactivity (25±8 Ci/μmol) at the end of the synthesis.

Human PET Studies

Healthy young volunteers aged 27–49 years (mean age 43.6±4.17 SEM, n=5) were recruited from the Baltimore Metropolitan area. All subjects received informed consent approved by the Johns Hopkins School of Medicine Investigational Review Board. Imaging studies were preceded by appropriate toxicology and safety studies including radiation dosimetry carried out in mouse organ biodistribution studies resulting in an FDA-approved IND.

Subjects were screened for the absence of significant neuropsychiatric and medical disorders (the inclusion criteria included healthy volunteers between 18 and 65 years old and BMI between 18 and 30 kg/m^2 inclusive and the exclusion criteria included smoking, drug or alcohol dependence, and any use of acetylcholinesterase inhibitors or prior psychotropic drugs; see details in Supplemental material). Screening procedures included a complete medical and medication history, demography, physical exam [including height, weight, and

body mass index (BMI)], vital signs, 12-lead electrocardiogram (ECG), and laboratory safety tests. All subjects agreed to receive a radial arterial line for blood sampling.

PET Imaging Procedures

Subjects were instructed not to ingest any alcohol, drugs, or over-the-counter medications for 48 h prior to PET scans and to arrive at JHU PET Center approximately 2–3 h before the scheduled first tracer injection time. Laboratory studies upon arrival included a urine toxicology screen, alcohol breathalyzer test, urine cotinine test, hematology, chemistry panel, and urine pregnancy screen for women. PET studies were performed on the high resolution research tomograph (HRRT) (Siemens)—the highest resolution (<2 mm) commercially available dedicated human brain PET scanner. A radial arterial catheter was used to obtain samples for plasma radioactivity for the kinetic model input function. An intravenous catheter was inserted into the antecubital vein for blood sampling and ligand injection. Each subject was fitted with a thermoplastic mask modeled to his or her face to reduce head motion during the PET study. A 6-min attenuation scan was performed using a rotating Cs-137 point source.

Each subject was carefully monitored for subjective symptoms throughout the procedure. Vital signs were obtained pre-injection and at 15, 30, 60, 90, and 120 min post-injection. A 3-lead ECG was performed throughout the scan, with 12-lead ECG obtained pre-injection and at 90 min post-injection after scanning was completed.

The emission scan began with a bolus (about 1 min) injection of [^{18}F]ASEM and lasted 90 min in a 3-D list mode. Five male subjects were injected with 13.9–16.2 mCi (15.1± 6.7 mCi; mean±SEM) with a mass ASEM dose of 0.20–0.67 mcg (0.35±0.15 mcg; mean±SEM) and specific activity of 8,000–27,300 mCi/μmol (18,600±8,300 mCi/μmol; mean± SEM). Arterial blood samples were obtained throughout the 90-min scan (approximately every 5 s initially and increasing to every 5 min after 30 min). Samples were centrifuged at 1,200×*g*, and the radioactivity in plasma was measured with a cross-calibrated gamma counter. Selected plasma samples (0, 2, 5, 10, 20, 30, 45, 60, and 90 min samples) were analyzed with high pressure liquid chromatography (HPLC) for radioactive metabolites in plasma, as described previously for baboon studies [34].

Reconstruction of Emission Scan

PET images were reconstructed in list mode using the iterative ordered subset expectation-maximization (OSEM) algorithm with 6 iterations, 16 subsets, data-mashing (span) of 3, and maximum ring difference of 67 and correcting for attenuation, scatter, and deadtime. The following frame sequence was used: four 15-s, four 30-s, three 1-min, two 2-min, five 4-min, and twelve 5-min frames or a total of 30 frames for the 90-min scan. The radioactivity was corrected for physical decay to the injection time. Each PET frame consists of 256 (left-to-right) by 256 (nasion-to-inion) by 207 (neck-to-cranium) voxels.

MR Imaging Procedures

Structural magnetic resonance (MR) of the brain was obtained to define volumes of interest (VOIs) and for gray and white matter segmentation. All MR imaging was done on the Siemens 3T TRIO at the B17 software level.

PET Data Analysis

VOIs—VOIs were defined automatically on individual subjects' SPGR MRI volumes using FSL's (The FMRIB Software Library [35]) FIRST tool [36] for subcortical regions and the Freesurfer tool [37] for cortical regions. Those automated VOIs were manually edited to fit the structures of interest using a locally developed VOI tool (VOILand). Refined VOIs were transferred from MRI to PET spaces according to MRI to PET co-registration parameters that were obtained by the co-registration module of SPM12 [38]. The VOIs in PET space were applied to PET frames to obtain time-activity curves (TACs) of various brain regions. Head motion correction (HMC) was performed using the co-registration module of SPM12 and/or the HRRT reconstruction head movement correction algorithm [39].

Derivation of the Outcome Variable, Distribution Volume (V_T), and Binding Potential (BP_{ND}) Using Human Reference Tissue (see below)—Standard compartmental models including one tissue (OTCM) and two tissue without (TTCM) and with (TTCMC) constraining the K_1/k_2 ratio (K_1 and k_2 are blood-brain and fractional brain-blood clearance constants) to the observed value of a low-receptor region were tested. Non-compartmental plasma reference graphical analysis (PRGA [40]) was tested for whether the kinetic behavior of [^{18}F]ASEM follows underlying assumptions of this model for radioligands with measurable dissociation (*i.e.*, PRGA plots of region reach asymptotes sometime after the tracer injection, often denoted as t*) within 10 min of the radiotracer injection). In these analyses, metabolite-corrected plasma TACs were obtained by applying the metabolite-corrected input function given by HPLC analysis to total plasma TACs after interpolating at plasma sample times using the piecewise cubic Hermite interpolation implemented in MATLAB (Cambridge, MA, USA).

Mouse Biodistribution Studies

Whole Body Mouse Regional Distribution—Distributions of activity were determined in male CD1 mice (26–28 g) after injection of [^{18}F]ASEM. Radioactivity concentrations were measured in various organs at six times up to 3-h post-injection in three animals per time point. This report summarizes radiation dose estimates for this agent based on these biokinetic data. The raw data for many tissues was presented in percent/organ and were assumed to be the same in humans. Values of percent of injected activity per organ were fit using the SAAM II software [41]. Time integrals of activity [42] were entered into the OLINDA/EXM software [43] using the adult male model. Greatest radioactivity was observed in the urinary bladder. The number of disintegrations in the 'remainder of the body' was assumed to be equal to 100 % of the activity administered integrated to total decay of ^{18}F minus the disintegrations in other body organs.

Brain Mouse Regional Distribution

Mouse brain regional distribution studies of [^{18}F]ASEM with and without administration of clinical α7-nAChR drugs were performed in CD1 male mice (n=4/per group, weight=25–27 g).

The dose escalation blocking studies in mice were performed by IP administration of DMXB-A (0.1 ml in saline) at 45 min after the IV injection of [^{18}F]ASEM (70 μCi, specific activity=11,000 mCi/μmol, 0.2 ml). Doses of DMXB-A were 0 (vehicle), 0.1, 0.3, 1, 3, 10, and 25 mg/kg in water. Note that the estimated equivalent dose in mice (25 mg/kg) corresponds [44] to the clinical dose (150 mg, oral) with understanding of the difference in the route of administration. Four animals per dose were used. At 90 min after administration of the radiotracer, the animals were euthanized, brain tissues were harvested and assayed in a γ-counter, and the brain regional radioactivity content was determined as percentage injected dose per gram (%ID/g) of tissue (mean±SD).

As a comparator, two other nicotinic drugs in clinical trials that bind at α7-nAChR, EVP-6124 [45], and varenicline [46] were co-injected IV with [^{18}F]ASEM (0.2 ml) into other groups of CD1 mice (n=4 per group). Both doses of EVP-6124 and varenicline were 0.18 mg/kg in water (0.1 ml), which corresponds to the estimated equivalent dose of the clinical dose (1 mg, oral). The animals were euthanized at 60 min post-injection, and the radioactivity in the brain regions was determined as described above for DMXB-A.

Results

Human Safety Studies

The mouse radiation dosimetry studies resulted in an estimated effective dose of 0.017 mSv/MBq (0.063 rem/mCi).

Human PET Studies

[^{18}F]ASEM readily entered the human brain (Fig. 2) after a bolus injection and demonstrated reversible kinetics with a peak (%SUV=400) at 10–15 min (Fig. 3). The regional brain distribution of [^{18}F]ASEM was comparable to the post-mortem data in the human brain [47, 48] and was similar to the distribution of [^{18}F]ASEM in the baboon brain [34].

The OTCM, TTCM, and TTCMC fit observed tissue and plasma TACs sufficiently well without showing systematic deviations of normalized residues (the residue over observed radioactivity averaged across subjects <5 %) at individual frames in all regions. Akaike information criterion [49] values were not different among the three methods (t<0.67; p>0.68), indicating that the goodness of fits were statistically indistinguishable when differences in numbers of parameters were taken into consideration. Using all frames (0–90 min), V_T values of the three methods correlated well (OTCM = 0.92·TTCM + 1.89; R^2 = 0.878; TTCMC = 1.0·TTCM−0.6; R^2=0.910) excluding one outlier (V_T > 60 ml/ml) observed with TTCM. Estimates of V_T were stable after 60 min (R^2>0.827; 0–60 *versus* 0–90 min) in the three methods excluding the outlier. Altogether (no outliers and a better time

consistency), TTCMC appeared to be the most appropriate among compartmental models. PRGA plots reached asymptotes by 10 min in all regions (R^2> 0.97) as we observed in our pre-clinical study in the baboon brain [34]. Estimates of V_T were stable after 60 min (V_T[60 min]=0.98·V_T[90 min]+0.05; R^2=0.969). Showing a better time consistency, PRGA appeared to be appropriate for [^{18}F]ASEM over compartmental models and was used for these results.

At present, it is not clear whether a reference region (*i.e.*, receptor free) exists for α7-nAChRs. White matter regions such as corpus callosum (CC) showed the lowest accumulation of [^{18}F]ASEM. If we use the CC as a reference tissue region, BP_{ND} [50] may be obtained by the (target V_T/reference V_T)−l. Precuneus, parietal, occipital, and cingulate cortices and putamen showed relatively high values of V_T (>20 ml/ml) and binding potential (BP_{ND}~1) while entorhinal cortex, cerebellum, caudate, and CC showed lower values of V_T (<15 ml/ml) (Fig. 4).

The test-retest variability (TRV) averaged at 10.8±5.1 % for medium and high V_T regions for the two subjects which were completed with two scans separated by a few days.

[^{18}F]ASEM Metabolite Analysis in Human Plasma

[^{18}F]ASEM was metabolized in the body to polar radiometabolites at rates comparable to other PET radioligands for CNS receptors. Reverse phase HPLC analysis demonstrated that all human [^{18}F]ASEM radiometabolites were the same as those in baboon plasma [34]. At 30 min and at 90 min, 52.6±12.9 and 83.5±9.7 %, respectively, of parent [^{18}F]ASEM was metabolized (Fig 5a). Plasma TACs peaked within 1 min (Fig. 5b). Thereafter, metabolite-corrected TACs declined mono-exponentially while total TACs started to increase gradually after 20 min, suggesting initial distribution of [^{18}F]ASEM to various organs and subsequent re-entry of its metabolites to the circulation.

Mouse Biodistribution Studies with Blockade Using Human Equivalent Doses of DMXB-A (GTS-21)

[^{18}F]ASEM binding in the α7-nAChR-rich brain regions was blocked in a dose-dependent fashion by DMXB-A (Fig. 6). The blockade was significant at a mouse-equivalent dose [44] comparable to the clinical dose of DMXB-A (25 mg/kg) and two lower doses (3 and 10 mg/kg), but it was not significant at the lowest doses (0.1–1 mg/kg). Specifically, at a dose of 25 mg/kg, DMXB-A significantly blocked [^{18}F]ASEM binding by 50–60 % in the hippocampus, cortex, and superior and inferior colliculus (p<0.01). The lower dose of 10 mg/kg showed similar levels (50–70 %) of blockade in the hippocampus, cortex, and subcolliculus (p<0.01). At the dose of 3 mg/kg, the observed blockade was smaller—28 % in the hippocampus (p<0.05) and 40 % in the cortex (p<0.05). The lowest doses of 0.1, 0.3, and 1 mg/kg did not show significant blockade.

Similar significant blockade of [^{18}F]ASEM was observed with two other nicotinic drugs in clinical trials that bind to the α7-nAChR, EVP-6124 [45], and varenicline [46] (Fig. 6). Both EVP-6124 and varenicline at a dose of 0.18 mg/kg (equivalent to the clinical dose of 1 mg/kg) blocked ASEM binding by 40–60 % in the hippocampus and cortex (p<0.05).

Discussion

As part of our PET radiotracer development program, we recently developed [^{18}F]ASEM (3-(1,4-diazabicyclo[3.2.2]nonan-4-yl)-6-[^{18}F]fluorodibenzo[*b,d*]thiophene 5,5-dioxide), a new highly specific PET radioligand for imaging of α7-nAChR [33, 34] (Fig. 1). *In vitro* [^{18}F]ASEM selectively binds at α7-nAChR with subnanomolar binding affinity (rat K_i =0.4 nM; human K_i = 0.3 nM) that is one to two orders of magnitude better than those of the previous best α7-nAChR PET tracers ([^{11}C]NS14492, [^{11}C]NS10743, and [^{18}F]AZ11637326) [33]. In addition, the α7-nAChR inhibition binding affinity of [^{18}F]ASEM is substantially better than that of its structural *para*-isomer 4-(8-[^{18}F]fluorodibenzo[b,d]thiophen-3-yl)-1,4-diazabicyclo[3.2.2]nonane 5,5-dioxide [^{18}F]*para*-ASEM (K_i=1.3 nM) [33]. After the original publication of [^{18}F]*para*-ASEM [33], this poorer affinity ligand was selected by others under a different name [51] as a potential PET tracer despite its less than optimal properties.

In vivo studies showed that [^{18}F]ASEM readily entered the mouse and baboon brains and specifically and selectively labeled cerebral α7-nAChR receptors [33, 34]. The binding potential BP_{ND} values of [^{18}F]ASEM in the mouse brain regions rich in α7-nAChR such as the cortex, hippocampus, and colliculus were BP_{ND} =5.3, 5.5, and 8.0, respectively. In the baboon brain, [^{18}F]ASEM exhibited BP_{ND} values of 3.9–6.6 [34]. The BP_{ND} values for [^{18}F]ASEM were at least 10 times greater than those of all previously published α7-nAChR PET radioligands [33].

PET Imaging of α7-nAChR with [^{18}F]ASEM

The kinetic characteristics of [^{18}F]ASEM of the five subjects are quite promising, with reversible binding within 90 min and with the advantages of higher resolution and the imaging statistics of the F-18 radiolabel. Regional binding is consistent with post-mortem human α7-nAChR brain distribution with the precuneus, parietal, occipital, and cingulate cortices and putamen showing higher values of V_T (>20 ml/ml) and with the entorhinal cortex, cerebellum, caudate, and CC showing lower values of V_T (<15 ml/ml). While only two of the five subjects had test-retest, the preliminary results of an average TRV of about 10–11 % were reasonable, but have to be confirmed with a larger sample size. The plasma metabolism was nearly 80–90 % by 90 min allowing a sufficient characterization of the input function. These imaging properties together with the reversible binding allowed similar results from a number of compartmental models, with the PRGA being the current choice in this preliminary study.

While it is premature to conclude that the CC can be a reliable reference region in the human brain, it was the lowest binding region and gave the higher binding regions a binding potential (BP_{ND}~1). The use of the CC as a reference region will be explored in future studies with larger numbers of subjects and with future human occupancy studies with α7-nAChR agonists such as DMXB-A.

Thus, our initial human PET studies provide evidence of the great potential for this radiotracer to image both α7-nAChR decrements (as expected in SCZ, traumatic brain injury, and Alzheimer’s disease) and increases (as may occur in bipolar disorder).

Potential for [^{18}F]ASEM Occupancy Studies

The critical role of the α7-nAChR in human physiology has recently been supported by clinical studies with α7-nAChR agonists—emerging drugs for treatment of cognitive dysfunction [13, 14]. Several drugs that target α7-nAChRs are now in the various clinical phases of development for numerous pathologies [8, 52]. Dimethoxybenzylidene anabaseine (DMXB-A or GTS-21) was the first selective α7-nAChR agonist that demonstrated cognitive enhancement in patients with SCZ [53, 54]. Currently, DMXB-A is in clinical trials for treatment of SCZ and other disorders.

Our prior rodent biodistribution studies used SSR180711, which successfully blocked [^{18}F]ASEM binding in both mouse and baboon brain, but clinical trials of SSR180711 were terminated in part due to insufficient efficacy and unacceptable side effects. Here, we have presented evidence for blockade in the mice brain with DMXB-A and measurable blockade with the α7-nAChR partial agonist EVP-6124 [45] and varenicline, which binds at two main CNS nAChR subtypes, α7-nAChR and α4β2 [46]. Both EVP-6124 [45] and varenicline are currently and have been previously used in clinical trials. This demonstrates the definitive feasibility of [^{18}F]ASEM for human α7-nAChR target engagement (by measuring the degree of receptor occupancy) to facilitate treatment strategies and opens new horizons for studying the biochemical mechanism of drugs for treatment of cognitive deficits in patients with SCZ.

Conclusions

[^{18}F]ASEM has enabled us to perform the first successful human PET studies of the α7-nAChR. The studies show suitable brain uptake with an appropriate regional distribution, matching the post-mortem results, and high, reversible binding sufficient for interrogating neuropsychiatric disorders *in vivo*. The *in vivo* rodent studies demonstrate the feasibility to measure receptor occupancy (and have target engagement) of clinical α7-nAChR drugs in a dose-dependent manner.

Supplementary Material

Refer to Web version on PubMed Central for supplementary material.

Acknowledgments

The authors received NIH grants MH079017 and AG037298 and funds from the Department of Radiology. Special thanks to Ali Kargbo, MS; Rebecca Mellinger Pilgram, BS; and Anil Mathur, MD, MIS for the HPLC metabolite analysis; Paige Finley, BS for the mouse experiments; the JHU PET technologists and PET radiochemists and Andrew Crabb, MS and Arman Rahmim, PhD for the computer-related and HRRT PET assistance. Thanks to Michael Stabin, PhD for assisting in radiation dosimetry estimates and Julia Buchanan for the editorial assistance.

References

1. Albuquerque EX, Pereira EF, Alkondon M, Rogers SW. Mammalian nicotinic acetylcholine receptors: from structure to function. Physiol Rev. 2009; 89:73–120. [PubMed: 19126755]
2. Philip NS, Carpenter LL, Tyrka AR, Price LH. Nicotinic acetylcholine receptors and depression: a review of the preclinical and clinical literature. Psychopharmacol (Berl). 2010; 212:1–12.

3. Ishikawa M, Hashimoto K. alpha7 nicotinic acetylcholine receptor as a potential therapeutic target for schizophrenia. Curr Pharm Des. 2011; 17:121–129. [PubMed: 21355839]
4. Parri HR, Hernandez CM, Dineley KT. Research update: alpha7 nicotinic acetylcholine receptor mechanisms in Alzheimer's disease. Biochem Pharmacol. 2011; 82:931–942. [PubMed: 21763291]
5. Woodruff-Pak DS, Gould TJ. Neuronal nicotinic acetylcholine receptors: involvement in Alzheimer's disease and schizophrenia. Behav Cogn Neurosci Rev. 2002; 1:5–20. [PubMed: 17715584]
6. D'Hoedt D, Bertrand D. Nicotinic acetylcholine receptors: an overview on drug discovery. Expert Opin Ther Targets. 2009; 13:395–411. [PubMed: 19335063]
7. Hoffmeister PG, Donat CK, Schuhmann MU, et al. Traumatic brain injury elicits similar alterations in alpha7 nicotinic receptor density in two different experimental models. Neruomol Med. 2011; 13:44–53.
8. Taly A, Charon S. Alpha7 nicotinic acetylcholine receptors: a therapeutic target in the structure era. Curr Drug Targets. 2012; 13:695–706. [PubMed: 22300037]
9. Freedman R, Hall M, Adler LE, Leonard S. Evidence in postmortem brain tissue for decreased numbers of hippocampal nicotinic receptors in schizophrenia. Biol Psychiatry. 1995; 38:22–33. [PubMed: 7548469]
10. Marutle A, Zhang X, Court J, et al. Laminar distribution of nicotinic receptor subtypes in cortical regions in schizophrenia. J Chem Neuroanat. 2001; 22:115–126. [PubMed: 11470559]
11. Thomsen MS, Weyn A, Mikkelsen JD. Hippocampal alpha7 nicotinic acetylcholine receptor levels in patients with schizophrenia, bipolar disorder, or major depressive disorder. Bipolar Disord. 2011; 13:701–707. [PubMed: 22085484]
12. Thomsen MS, Hansen HH, Timmerman DB, Mikkelsen JD. Cognitive improvement by activation of alpha7 nicotinic acetylcholine receptors: from animal models to human pathophysiology. Curr Pharm Des. 2010; 16:323–343. [PubMed: 20109142]
13. Olincy A, Freedman R. Nicotinic mechanisms in the treatment of psychotic disorders: a focus on the alpha7 nicotinic receptor. Handb Exp Pharmacol. 2012; 213:211–232.
14. Mazurov AA, Speake JD, Yohannes D. Discovery and development of alpha7 nicotinic acetylcholine receptor modulators. J Med Chem. 2011; 54:7943–7961. [PubMed: 21919481]
15. Kulak JM, Schneider JS. Differences in alpha7 nicotinic acetylcholine receptor binding in motor symptomatic and asymptomatic MPTP-treated monkeys. Brain Res. 2004; 999:193–202. [PubMed: 14759498]
16. Kulak JM, Carroll FI, Schneider JS. [125I]Iodomethyllycaconitine binds to alpha7 nicotinic acetylcholine receptors in monkey brain. Eur J Neurosci. 2006; 23:2604–2610. [PubMed: 16817863]
17. Horti AG, Villemagne VL. The quest for Eldorado: development of radioligands for *in vivo* imaging of nicotinic acetylcholine receptors in human brain. Curr Pharm Des. 2006; 12:3877–3900. [PubMed: 17073685]
18. Toyohara J, Wu J, Hashimoto K. Recent development of radioligands for imaging alpha7 nicotinic acetylcholine receptors in the brain. Curr Top Med Chem. 2010; 10:1544–1557. [PubMed: 20583992]
19. Brust P, Peters D, Deuther-Conrad W. Development of radioligands for the imaging of alpha7 nicotinic acetylcholine receptors with positron emission tomography. Curr Drug Targets. 2012; 13:594–601. [PubMed: 22300025]
20. Pomper MG, Phillips E, Fan H, et al. Synthesis and biodistribution of radiolabeled alpha 7 nicotinic acetylcholine receptor ligands. J Nucl Med. 2005; 46:326–334. [PubMed: 15695794]
21. Hashimoto K, Nishiyama S, Ohba H, et al. [11C]CHIBA-1001 as a novel PET ligand for alpha7 nicotinic receptors in the brain: a PET study in conscious monkeys. PLoS One. 2008; 3:e3231. [PubMed: 18800169]
22. Ogawa M, Nishiyama S, Tsukada H, et al. Synthesis and evaluation of new imaging agent for central nicotinic acetylcholine receptor alpha7 subtype. Nucl Med Biol. 2010; 37:347–355. [PubMed: 20346874]
23. Dolle F, Valette H, Hinnen F, et al. Synthesis and preliminary evaluation of a carbon-11-labelled agonist of the a7 nicotinic acetylcholine receptor. J Label Compd Radiopharm. 2001; 44:785–795.

24. Toyohara J, Ishiwata K, Sakata M, et al. *In vivo* evaluation of alpha7 nicotinic acetylcholine receptor agonists [^{11}C]A-582941 and [11C]A-844606 in mice and conscious monkeys. PLoS One. 2010; 5:e8961. [PubMed: 20126539]
25. Horti AG, Ravert HT, Gao Y, et al. Synthesis and evaluation of new radioligands [(11)C]A-833834 and [(11)C]A-752274 for positron-emission tomography of alpha7-nicotinic acetylcholine receptors. Nucl Med Biol. 2013; 40:395–402. [PubMed: 23294899]
26. Gao Y, Ravert HT, Valentine H, et al. 5-(5-(6-[(11)C]methyl-3,6-diazabicyclo[3.2.0]heptan-3-yl)pyridin-2-yl)-1H-indole as a potential PET radioligand for imaging cerebral alpha7-nAChR in mice. Bioorg Med Chem. 2012; 20:3698–3702. [PubMed: 22608919]
27. Toyohara J, Sakata M, Wu J, et al. Preclinical and the first clinical studies on [11C]CHIBA-1001 for mapping alpha7 nicotinic receptors by positron emission tomography. Ann Nucl Med. 2009; 23:301–309. [PubMed: 19337782]
28. Peters D, Timmerman DB, Roenn LC, Nielsen EB. Preparation of labeled indolyl-pyridazinyl-diazabicyclononane derivatives and their use in diagnostic methods, particularly receptor imaging. 2009
29. Deuther-Conrad W, Fischer S, Hiller A, et al. Assessment of alpha7 nicotinic acetylcholine receptor availability in juvenile pig brain with [^{18}F]NS10743. Eur J Nucl Med Mol Imaging. 2011; 38:1541–1549. [PubMed: 21484373]
30. Ettrup A, Mikkelsen JD, Lehel S, et al. 11C–NS14492 as a novel PET radioligand for imaging cerebral alpha7 nicotinic acetylcholine receptors: *in vivo* evaluation and drug occupancy measurements. J Nucl Med. 2011; 52:1449–1456. [PubMed: 21828113]
31. Tanibuchi Y, Wu J, Toyohara J, et al. Characterization of [(3)H]CHIBA-1001 binding to alpha7 nicotinic acetylcholine receptors in the brain from rat, monkey, and human. Brain Res. 2010; 1348:200–208. [PubMed: 20537987]
32. Ding M, Ghanekar S, Elmore CS, et al. [^{3}H]Chiba-1001 (methyl-SSR180711) has low *in vitro* binding affinity and poor *in vivo* selectivity to nicotinic alpha-7 receptor in rodent brain. Synapse. 2012; 66:315–322. [PubMed: 22108786]
33. Gao Y, Kellar KJ, Yasuda RP, et al. Derivatives of dibenzothiophene for positron emission tomography imaging of alpha7-nicotinic acetylcholine receptors. J Med Chem. 2013; 56:7574–7589. [PubMed: 24050653]
34. Horti AG, Gao Y, Kuwabara H, et al. ^{18}F-ASEM, a radiolabeled antagonist for imaging the alpha7-Nicotinic acetylcholine receptor with PET. J Nucl Med. 2014; 55:672–677. [PubMed: 24556591]
35. Jenkinson M, Beckmann CF, Behrens TE, Woolrich MW, Smith SM. Fsl. Neuroimage. 2012; 62:782–790. [PubMed: 21979382]
36. Patenaude B, Smith SM, Kennedy DN, Jenkinson M. A Bayesian model of shape and appearance for subcortical brain segmentation. Neuroimage. 2011; 56:907–922. [PubMed: 21352927]
37. Fischl B, van der Kouwe A, Destrieux C, et al. Automatically parcellating the human cerebral cortex. Cereb Cortex. 2004; 14:11–22. [PubMed: 14654453]
38. Ashburner, J., Friston, KJ. Rigid body registration. In: Frackowiak, R.Ashburner, J.Penny, WD., et al., editors. Human brain function. Academic; San Diego: 2004. p. 635-654.
39. Keller SH, Sibomana M, Olesen OV, et al. Methods for motion correction evaluation using 18F-FDG human brain scans on a high-resolution PET scanner. J Nucl Med. 2012; 53:495–504. [PubMed: 22331217]
40. Logan J, Fowler JS, Volkow ND, et al. Distribution volume ratios without blood sampling from graphical analysis of PET data. J Cereb Blood Flow Metab. 1996; 16:834–840. [PubMed: 8784228]
41. Foster DM. Developing and testing integrated multicompartment models to describe a single-input multiple-output study using the SAAM II software system. Adv Exp Med Biol. 1998; 445:59–78. [PubMed: 9781382]
42. Stabin MG, Siegel JA. Physical models and dose factors for use in internal dose assessment. Health Phys. 2003; 85:294–310. [PubMed: 12938720]
43. Stabin MG, Sparks RB, Crowe E. OLINDA/EXM: the second-generation personal computer software for internal dose assessment in nuclear medicine. J Nucl Med. 2005; 46:1023–1027. [PubMed: 15937315]

44. Reagan-Shaw S, Nihal M, Ahmad N. Dose translation from animal to human studies revisited. FASEB J. 2008; 22:659–661. [PubMed: 17942826]
45. Prickaerts J, van Goethem NP, Chesworth R, et al. EVP-6124, a novel and selective alpha7 nicotinic acetylcholine receptor partial agonist, improves memory performance by potentiating the acetylcholine response of alpha7 nicotinic acetylcholine receptors. Neuropharmacology. 2012; 62:1099–1110. [PubMed: 22085888]
46. Rollema H, Shrikhande A, Ward KM, et al. Pre-clinical properties of the alpha4beta2 nicotinic acetylcholine receptor partial agonists varenicline, cytisine and dianicline translate to clinical efficacy for nicotine dependence. Br J Pharmacol. 2010; 160:334–345. [PubMed: 20331614]
47. Court JA, Martin-Ruiz C, Graham A, Perry E. Nicotinic receptors in human brain: topography and pathology. J Chem Neuroanat. 2000; 20:281–298. [PubMed: 11207426]
48. Breese CR, Adams C, Logel J, et al. Comparison of the regional expression of nicotinic acetylcholine receptor alpha7 mRNA and [^{125}I]-alpha-bungarotoxin binding in human postmortem brain. J Comp Neurol. 1997; 387:385–398. [PubMed: 9335422]
49. Akaike H. A new look at statistical model identification. IEEE Trans Autom Control. 1974; AU-19:716–722.
50. Innis RB, Cunningham VJ, Delforge J, et al. Consensus nomenclature for *in vivo* imaging of reversibly binding radioligands. J Cereb Blood Flow Metab. 2007; 27:1533–1539. [PubMed: 17519979]
51. Kranz M, Sattler B, Deuther-Conrad W, et al. Preclinical dose assessment and biodistribution of [^{18}F]DBT10, a new α7 nicotinic acetylcholine receptor (α7-nAChR) imaging ligand. J Nucl Med. 2014; 55(Suppl 1):1143.
52. Wallace TL, Bertrand D. Alpha7 neuronal nicotinic receptors as a drug target in schizophrenia. Expert Opin Ther Targets. 2013; 17:139–155. [PubMed: 23231385]
53. Freedman R, Olincy A, Buchanan RW, et al. Initial phase 2 trial of a nicotinic agonist in schizophrenia. Am J Psychiatry. 2008; 165:1040–1047. [PubMed: 18381905]
54. Olincy A, Harris JG, Johnson LL, et al. Proof-of-concept trial of an alpha7 nicotinic agonist in schizophrenia. Arch Gen Psychiatry. 2006; 63:630–638. [PubMed: 16754836]

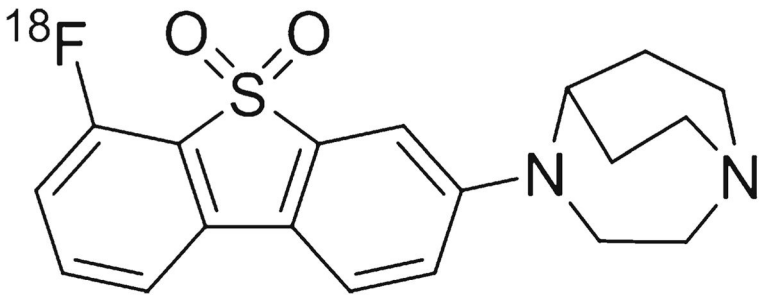

Fig. 1.
Chemical structure of [^{18}F]ASEM.

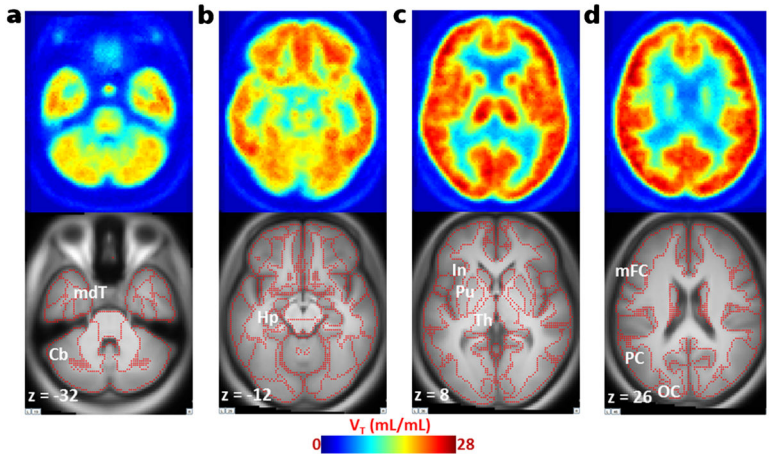

Fig. 2.

Averaged (n=5) transaxial images of spatially normalized V_T map of [^{18}F]ASEM and matching MRI in healthy control subjects. **a** Cerebellum (*Cb*) and medial temporal cortex (*mdT*) showed relatively low V_T values; **b** hippocampus (*Hp*) showed medium V_T values. **c** The insula (*In*), putamen (*Pu*), and thalamus (*Th*); **d** middle frontal (*mFC*), parietal (*PC*), and occipital (*OC*) cortices exhibited high V_T values in the human brain. *Red dots* on MRI images indicate outlines of cortical and subcortical structures.

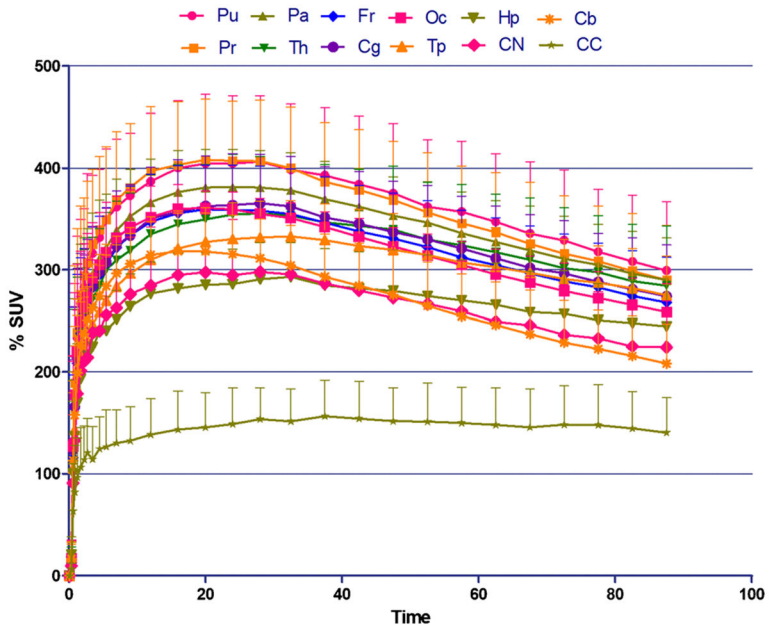

Fig. 3.

Baseline PET/[^{18}F]ASEM TAC [%SUV±SD (n=5)] in healthy human males. *Pu*, putamen; *Pr*, precuneus; *Pa*, parietal lobe; *Th*, thalamus; *Fr*, frontal lobe; *Cg*, cingulate; *Oc*, occipital; *Tp*, temporal lobe; *Hp*, hippocampus; *CN*, caudate nucleus; *Cb*, cerebellum; *CC*, corpus callosum. The distribution of [^{18}F]ASEM in the human brain regions is comparable with non-human primate (see, for review, [34]) and human post-mortem distribution of α7 [47, 48]. The brain kinetics of [^{18}F]ASEM is reversible.

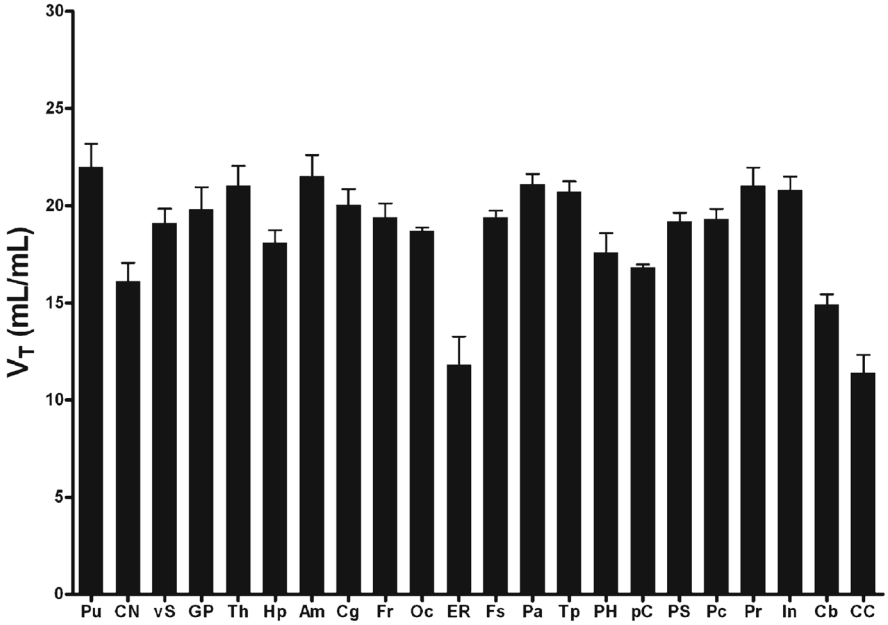

Fig. 4.

Histogram (mean±SD bar) of regional values of distribution volume (V_T) for selected human brain regions. Regions are putamen (*Pu*), caudate nucleus (*CN*), ventral striatum (*vS*), global pallidus (*GP*), thalamus (*Th*), hippocampus (*Hp*), amygdala (*Am*), cingulate (*Cg*), frontal lobe (*Fr*), occipital lobe (*Oc*), entorhinal area (*ER*), fusiform gyrus (*Fs*), parietal lobe (*Pa*), temporal lobe (*Tp*), parahippocampus (*PH*), paracentral (*pC*), post-central gyrus (*PS*), pre-central gyrus (*Pc*), precuneus (*Pr*), insula (*In*), cerebellum (*Cb*), corpus callosum (*CC*).

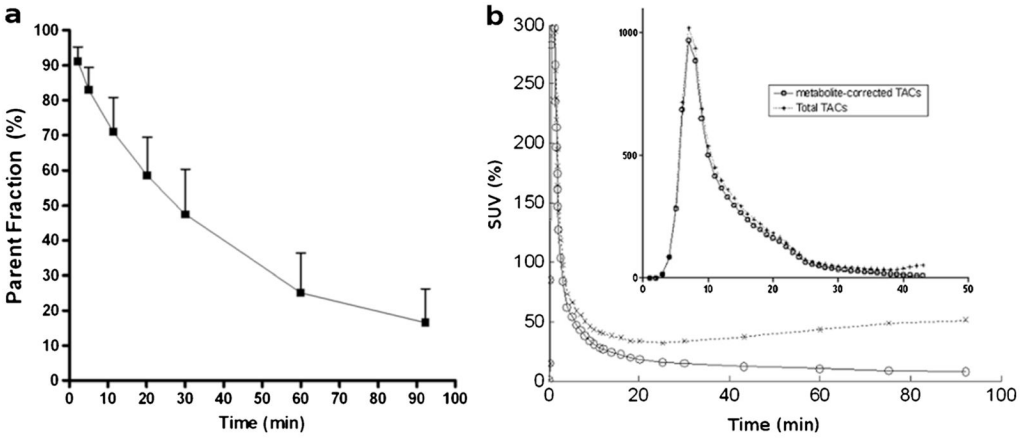

Fig. 5.

a Time-profile (mean of five subjects with one SD bars) of parent fraction [^{18}F]ASEM in plasma after the injection and **b** total and metabolite-corrected plasma time-activity curves (TACs; mean of five subjects) expressed in SUV with an insert showing plots in the first 5 min. Coefficients of variation (SD over mean expressed in percentage) ranged from 21.1 and 27.2 % (t>10 min) for metabolite-corrected TACs.

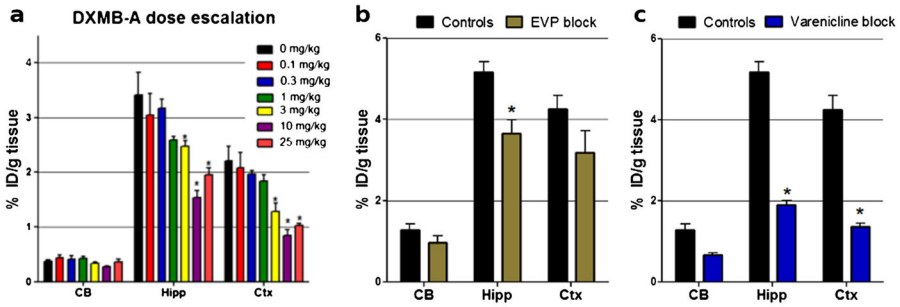

Fig. 6.

Baseline *versus* blockade studies of [^{18}F]ASEM with mouse-equivalent doses [44] of clinical α7-nAChR drugs in CD1 mice. Data: %ID/g tissue±SD (n=4). The control mice were treated with vehicle saline. *CB*, cerebellum; *Hipp*, hippocampus; *Ctx*, cortex. Statistics for all three drugs: *P<0.01, blockade is significantly different from controls (ANOVA). **a** DMXB-A (GTS-21), dose escalation. A mouse-equivalent dose=25 mg/kg of the clinical dose (150 mg). Ninety-min post-[^{18}F]ASEM injection. **b** EVP-6124, a mouse-equivalent dose (0.18 mg/kg) of the clinical dose (1 mg). Sixty-min post-[^{18}F]ASEM injection. **c** varenicline, a mouse-equivalent dose (0.18 mg/kg) of the clinical dose (1 mg). Sixty-min post-[^{18}F]ASEM injection. The graph demonstrates that *in vivo* binding of [^{18}F]ASEM in the mouse brain regions enriched with α7-nAChR is significantly blocked by the α7-nAChR drugs DMXB-A, EVP-6124, and varenicline.